Possible Organization for Writing a Thesis including a LaTeXFramework and Examples

by

A Graduate Advisor
B.Sc., University of WhoKnowsWhere, 2053
M.Sc., University of AnotherOne, 2054

A Dissertation Submitted in Partial Fulfillment of the
Requirements for the Degree of

DOCTOR OF PHILOSOPHY

in the Department of Whichever

Possible Organization for Writing a Thesis including a LaTeXFramework and Examples

by

A Graduate Advisor
B.Sc., University of WhoKnowsWhere, 2053
M.Sc., University of AnotherOne, 2054

Supervisory Committee

Dr. R. Supervisor Main, Supervisor
(Department of Same As Candidate)

Dr. M. Member One, Departmental Member
(Department of Same As Candidate)

Dr. Member Two, Departmental Member
(Department of Same As Candidate)

Dr. Outside Member, Outside Member
(Department of Not Same As Candidate)

Supervisory Committee

Dr. R. Supervisor Main, Supervisor
(Department of Same As Candidate)

Dr. M. Member One, Departmental Member
(Department of Same As Candidate)

Dr. Member Two, Departmental Member
(Department of Same As Candidate)

Dr. Outside Member, Outside Member
(Department of Not Same As Candidate)

ABSTRACT

This document is a possible Latex framework for a thesis or dissertation at UVic. It should work in the Windows, Mac and Unix environments. The content is based on the experience of one supervisor and graduate advisor. It explains the organization that can help write a thesis, especially in a scientific environment where the research contains experimental results as well. There is no claim that this is the *best* or *only* way to structure such a document. Yet in the majority of cases it serves extremely well as a sound basis which can be customized according to the requirements of the members of the supervisory committee and the topic of research. Additionally some examples on using LaTeXare included as a bonus for beginners.

Contents

List of Tables

List of Figures

ACKNOWLEDGEMENTS

I would like to thank:

my cat, Star Trek, and the weather, for supporting me in the low moments.

Supervisor Main, for mentoring, support, encouragement, and patience.

Grant Organization Name, for funding me with a Scholarship.

I believe I know the only cure, which is to make one's centre of life inside of one's self, not selfishly or excludingly, but with a kind of unassailable serenity-to decorate one's inner house so richly that one is content there, glad to welcome any one who wants to come and stay, but happy all the same in the hours when one is inevitably alone.

Edith Wharton

DEDICATION

Just hoping this is useful!

Chapter 1

Introduction

Chapter 2

Theory

The **Standard Model of Particle Physics (SM)** [15, 17, 12, 11] is a quantized relativistic field theory that describes all known elementary particles, as well as their interactions via three of the four known fundamental forces. It has been tested extremely rigorously since its development in the 1960s and 1970s, and in every case its predictions have held true. The final piece of the puzzle fell into place with the experimental verification of the existence of the Higgs Boson in 2012 [1].

Despite its success, however, the SM is considered an incomplete theory. It does not describe the interaction of matter via the fourth fundamental force, gravity, nor does it account for the existence of *dark matter* in our universe, or the asymmetry between the observed amounts matter and anti-matter. These shortcomings provide motivation to extend the SM by searching beyond it for new phenomena.

This chapter will provide a short overview of the SM theory, before describing some of the deficiencies that motivate an extension of it.

2.1 The Standard Model

2.1.1 The Particles

The elementary particles of the Standard Model are shown in Figure 2.1. They can be categorized into two groups: *fermions* and *bosons*. *Fermions* carry half-integer spin, and constitute the matter that surrounds us. For each fermion there also exists a corresponding anti-particle with an opposite electric charge. In this document anti-particles will be denoted either by the charge (e.g. e^+ vs. e^-) or by a bar overhead e.g. (t vs. $\bar{t}$). The fermions can be further divided into two groups: *leptons* and

quarks. *Leptons*, the most familiar of which is the electron, interact via the weak force and, if electrically charged, the electromagnetic force. They come in three flavour generations, each of which has a neutral particle (*neutrino*) and a charged fermion with electric charge -1. Unlike leptons, which regularly exist freely, *quarks* exist mostly in bound states called *hardrons*, the most well-know of which are the proton and neutron composed of (u, u, d) and (u, d, d) quarks respectively. Like leptons, quarks come in three generations, each of which has a pair of particles with electric charges +2/3 and -1/3. They interact via all three forces of the standard model: strong, weak, and electromagnetic.

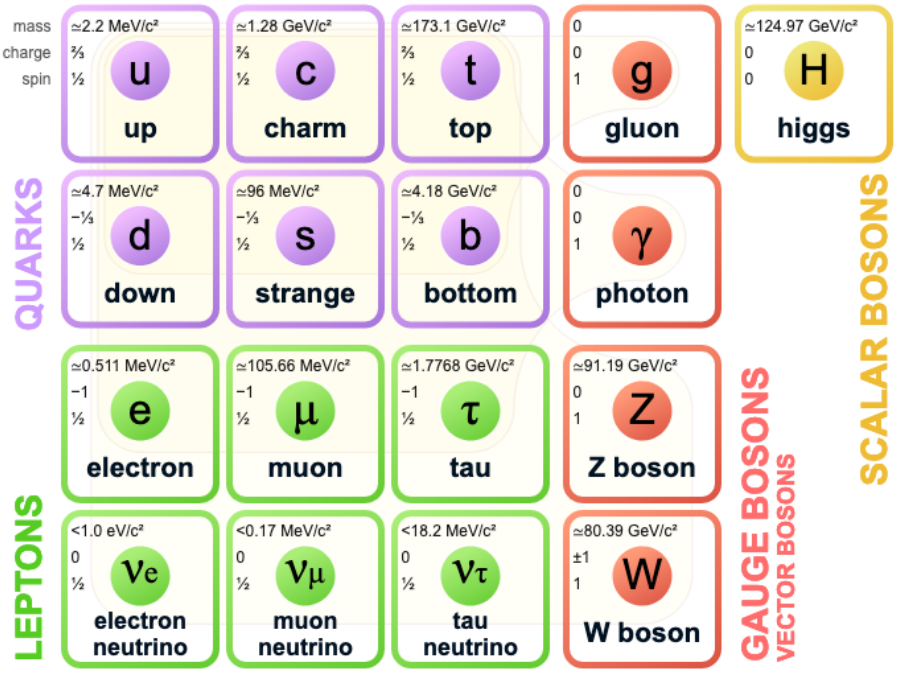

Figure 2.1: The elementary particles of the Standard Model

Bosons carry integer spin, and mediate the forces via which particles interact. Massless *gluons* and *photons* as well as massive W and Z bosons are spin-1 vector bosons, while the Higgs Boson is a spin-0 scalar boson. The massive W and Z vector bosons are the carriers of the weak force, the photon carries the electromagnetic force, and the gluons carry the strong force binding quarks. Along with interacting with fermions via exchange, bosons are also able to interact among themselves. W bosons are able to directly interact with both Z bosons and and photons, as well as self-interacting. Gluons can also self-interact, but Z bosons and photons cannot. The Higgs boson interacts with all massive particles, including self-interaction, and it is

via their interaction with the Higgs field that massive bosons obtain their mass.

2.1.2 Quantum Electrodynamics (QED)

Quantum Electrodynamics (QED) [8, 17, 15] is a quantum field theory of electrodynamics and the electromagnetic force. It describes the interaction of electrically charged particles via the exchange of photons. Mathematically, QED is an abelian (commutative) gauge theory with the gauge group $U(1)$. The fundamental interactions of the theory are: the emission or absorption of a single photon by a charged particle and the creation or annihilation of a pair of charged particles. These interactions can each be represented by various orientations of the Feynman vertex shown in Figure 2.2.

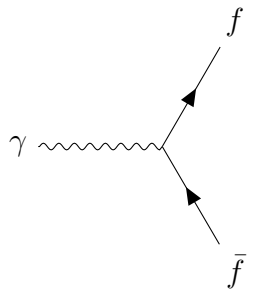

Figure 2.2: The fundamental QED vertex.

2.1.3 Weak Interactions

The weak force [12, 9, 10, 18], in contrast to the electromagnetic force, is mediated by the exchange of massive vector bosons W^+, W^-, and Z. Owing to the charge of the W bosons, and the fact in contrast to the electromagnetic force neutral fermions also interact via the weak force, there are many more possible fundamental interactions. Figure 2.3 shows the vertices corresponding three such interactions: fermions interacting with the Z boson in a similar vertex to that of Figure 2.2 shown in (a), a charged lepton and neutrino interacting with a W boson shown in (b), and a quark-antiquark pair interacting with a W boson shown in (c).

At high energy scales, the aforementioned electromagnetic force and the weak force unify to become the electroweak interaction. Glashow, Salam, and Weinberg's Electroweak theory unites the two forces into a single $U(1) \otimes SU(2)$ gauge theory.

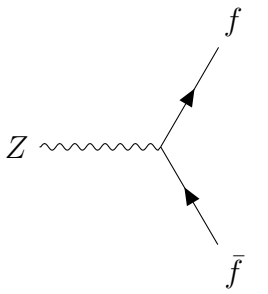

(a) Z interaction.

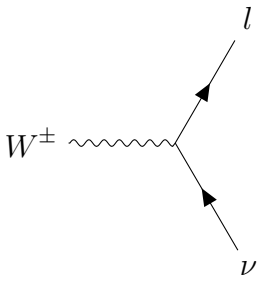

(b) W interaction with leptons.

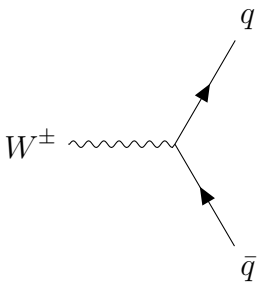

(c) W interaction with quarks.

Figure 2.3: Some fundamental weak interaction vertices.

2.1.4 Quantum Chromodynamics (QCD)

Quantum Chromodynamics (QCD) [12, 3] is the theory describing the strong interaction between gluons and quarks. It is again a gauge theory, this time with the SU(3) symmetry group. There are three colour charges associated with this group, which are carried by both quarks and gluons. Each of the 8 gluons carries a unique colour charge and anti colour charge pair, while quarks carry a single colour charge. Because they carry colour charge, gluons are able to both interact with quarks and self-interact. This gives rise to several possible interaction vertices in the theory, some of which are shown in Figure 2.4.

(a) Gluon interaction with quarks.

(b) Gluon self-interaction.

Figure 2.4: Some fundamental QCD interaction vertices.

2.1.5 The Higgs Boson

Electroweak theory alone does not contain a mechanism to provide particles with mass. This contrasts with the observed reality that all fermions as well as W and Z bosons are in fact massive. If the lagrangian of these theories were to contain mass terms, they would lose their gauge invariance and the standard model would not be renormalizable. Instead, these particles acquire their mass through the *Higgs Mechanism* [6, 13, 14].

A new Higgs Field Φ is introduced, with a Lagrangian which can be written as:

$$\mathcal{L}_{Higgs} = (D_\mu \Phi)^\dagger D^\mu \Phi + V(\Phi) \tag{2.1}$$

Where D_μ is the gauge covariant derivative of the electroweak theory. In order for the Lagrangian to remain gauge invariant the Higgs potential $V(\Phi)$ must take the form:

$$V(\Phi) = \mu^2 \Phi + \lambda \Phi^4 \tag{2.2}$$

where λ and Φ are free parameters. λ is forced to be greater than 0 by requiring that the potential have a stable minimum. This leads the potential to have two different possible shapes, shown in Figure 2.5, given the sign of μ^2:

1. $\mu^2 > 0$: The trivial case of a parabolic potential with a minimum at $\Phi = 0$ arises.

2. $\mu^2 > 0$: A potential with a minimum at:

$$|\Phi| = v = \sqrt{\frac{\mu^2}{\lambda}} \tag{2.3}$$

arises, where v is known as the vacuum expectation value. This minimum is occupied by infinitely degenerate states. This is the case that gives rise to the Higgs mechanism.

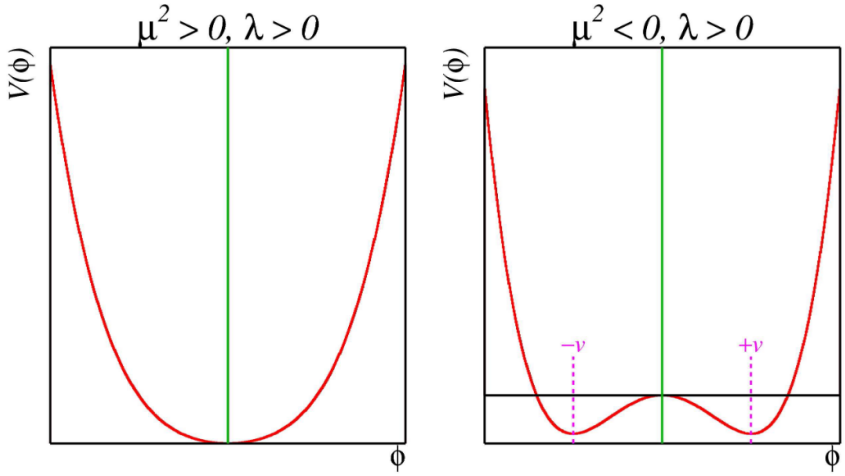

Figure 2.5: Shapes of the Higgs Potential for different cases of μ^2.

In the second case, the ground states occupying the minimum are not equivalent under gauge transformation, which breaks the Electroweak gauge symmetry. The masses of particles are then determined by the strength of their coupling to the Higgs field.

2.2 Beyond the Standard Model

The Standard Model as described above has proven extremely robust through precise experimental testing. There are, however, many remaining questions in physics that cannot be answered within its confines. Some of those not further explored in this thesis include: whether or not there is a quantum theory of gravity that can tie it to the SM, the exact value of the neutrino masses and whether they are Majorana particles (their own antiparticles), and what the cause is of the matter-antimatter

asymmetry in the universe. The fact that these questions are unanswered in the standard model tells us we must search deeper, and test beyond its limits.

2.2.1 Dark Matter

Another currently open question is the nature of dark matter. Astrophysical observations including the dynamics of galaxy clusters [19] and rotational curves of galaxies [16] are not explained under Einstein's theory of gravitation by visible matter alone. Several theories have arisen over time to explain this discrepancy, including that Einstein's theory is not correct at galactic scales, or that these galaxies contain ordinary matter that is somehow unobservable to us.

Most evidence, however, points to the existence of a new type of matter that interacts gravitationally but not electromagnetically with ordinary matter. Perhaps the most clear evidence for this theory comes from observations of the bullet cluster [4], a pair of colliding clusters of galaxies. In such a scenario, with some normal matter and some dark matter in each cluster, the matter would collide and interact, slowing it down, while the dark matter would pass through largely undisturbed. In the case of the bullet cluster, this separation is observed when comparing the distribution of mass in the galaxies measured by gravitational lensing and the distribution of normal matter in the form of galaxy plasma, measured as emitted x-ray radiation. Figure 2.6 shows the observed separation, with gravitational density in blue and x-ray density in pink.

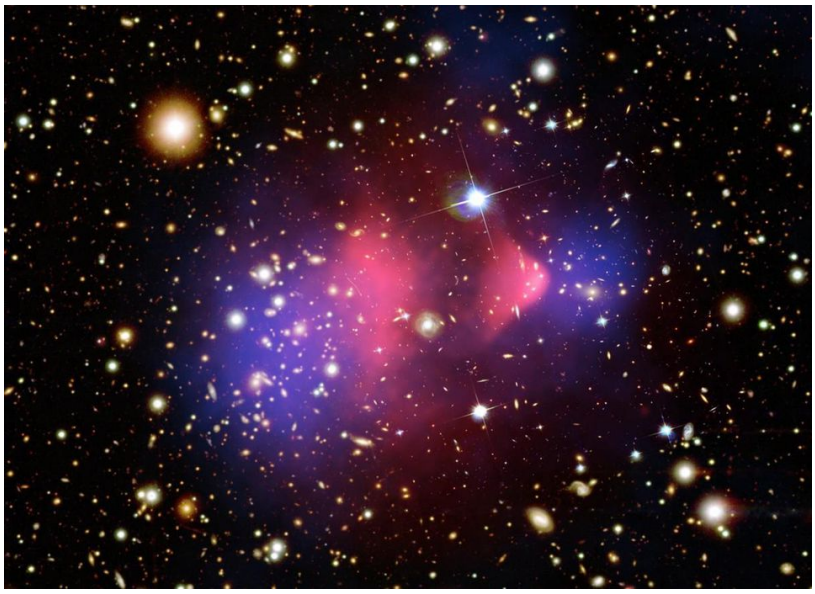

Figure 2.6: The bullet cluster showing separation of x-ray density (pink) and gravitational density (blue).

2.2.2 Dark Higgs Boson Model

This work involves a search for dark matter produced in association with a new hypothetical scalar "dark Higgs" boson s[1] [5]. In this model the dark matter particle χ is a majorana fermion, who's mass is generated by a Higgs mechanism in the dark sector. This also generates the new s particle. If the mass of s is less than that of χ then the relic density is set by the process $\chi\chi \to ss$, followed by the decay of s to standard model partices. The addition of a further paricle, such as a massive Z' boson allows this model to be probed at a collider.

The model proposes that the dark matter particle χ obtains its mass from the vacuum expectation value (vev) w of a new Higgs field S. A new $U(1)'$ gauge group is proposed, under which S carries a charge q_s. As a result, the vev w of S breaks the gauge symmetry, and through this mechanism the mass of the corresponding Z' boson is generated. Additionally, the dark matter particle χ couples to the Z' boson, allowing all particles in the new dark sector to interact. This gives rise to the renormalizable interaction Lagrangian, which can be written in terms of four independent parameters m_χ, $m_{Z'}$, m_s, and g_χ:

[1] In this work, s will refer to the dark Higgs boson and not the strange quark, unless otherwise spefcified

$$\mathcal{L}_\chi = -\frac{1}{2} g_\chi Z'^\mu \bar{\chi} \gamma^5 \gamma_\mu \chi - g_\chi \frac{m_\chi}{m_{Z'}} s \bar{\chi} \chi + 2 g_\chi Z'^\mu Z'_\mu (g_\chi s^2 + m_{Z'} s) \tag{2.4}$$

where m_χ is the mass of the dark matter particles, $m_{Z'}$ is the mass of the Z' boson, m_s is the mass of the dark higgs, and g_χ is the dark matter coupling constant.

Additionally, the coupling of the Z' boson to standard model quarks is described by the Lagrangian:

$$\mathcal{L} = -g_q Z'^\mu \bar{q} \gamma_\mu q \tag{2.5}$$

where g_q is the coupling constant between Z' and quarks.

A final free parameter θ is the non-zero mixing angle between the SM Higgs boson and the dark Higgs boson. The dark Higgs obtains its couplings to standard model particles through this mixing, and therefore shares the same standard model decay branching fractions as the SM Higgs boson.

For the analysis described in this work the free parameters are set as:

- $g_\chi = 1$
- $m_\chi = 200 GeV$
- $m_{Z'}$ allowed to vary
- m_s allowed to vary
- $g_q = 0.25$
- $\theta = 0.01$

The values of g_χ and g_q were chosen to facilitate comparison with other LHC searches with similar models, which traditionally use the values selected. The value of θ was chosen to match that of [5]. Its precise value is not relevant to this search, but it is sufficiently large that the dark Higgs decays promptly to standard model states and does not create a displaced vertex. The varied values m_s and $m_{Z'}$ form the parameter space covered by this search.

Chapter 3

The Large Hadron Collider and the ATLAS Experiment

The **Large Hadron Collider (LHC)** is the world's largest and most energetic proton-proton collider. It forms a 27 km circular ring beneath Switzerland and France, with its origin at the **Conseil Européen pour Recherche Nucléaire (CERN)** in Geneva. It began operation in 2008, and since then has collided over 10^{15} particles. The collider houses four major experiments: ALICE, ATLAS, CMS, and LHCb, along with several smaller projects. ALICE (A Large Ion Collider Experiment) studies heavy ion collisions, while LHCb (Large Hardon Collider beauty) specializes in studying the physics of the bottom quark. **ATLAS (A Toroidal LHC ApparatuS)** and CMS (Compact Muon Solenoid) are both general purpose experiments designed to study a wide range of interactions resulting from high-energy proton-proton collisions. This work uses data collected by the ATLAS experiment, and a description of the LHC accelerator and ATLAS detector follow in Sections 3.1 and 3.2.

3.1 The Large Hadron Collider

Built between 1998 and 2008, the LHC [7] began colliding protons in 2010 at a center-of-mass energy of 7 TeV, and most recently from 2015 to 2018 collisions occured at 13 TeV. Successfully colliding particles at this energy is an immense technical challenge which is achieved by the many technologies of the LHC and its accelerator complex.

In order to reach a beam energy of 6.5 TeV, protons are slowly stepped up through a chain of accelerators before reaching the LHC. They begin their journey as hydrogen

atoms, stripped of their electrons before being accelerated to an energy of 50 MeV by the Linac2 linear accelerator. Following this the Proton Synchrotron Booster (PSB) accelerates them to 1.4 GeV, passing them to the Proton Synchrotron (PS) and the Super Proton Synchrotron to be accelerated to 25 and then 450 GeV. Finally, beams are split into clockwise and counterclockwise directions and injected into the LHC where they are accelerated to their final 6.5 TeV energy. The CERN accelerator complex, including this injection system as well as surrounding experiments is shown in Figure 3.1.

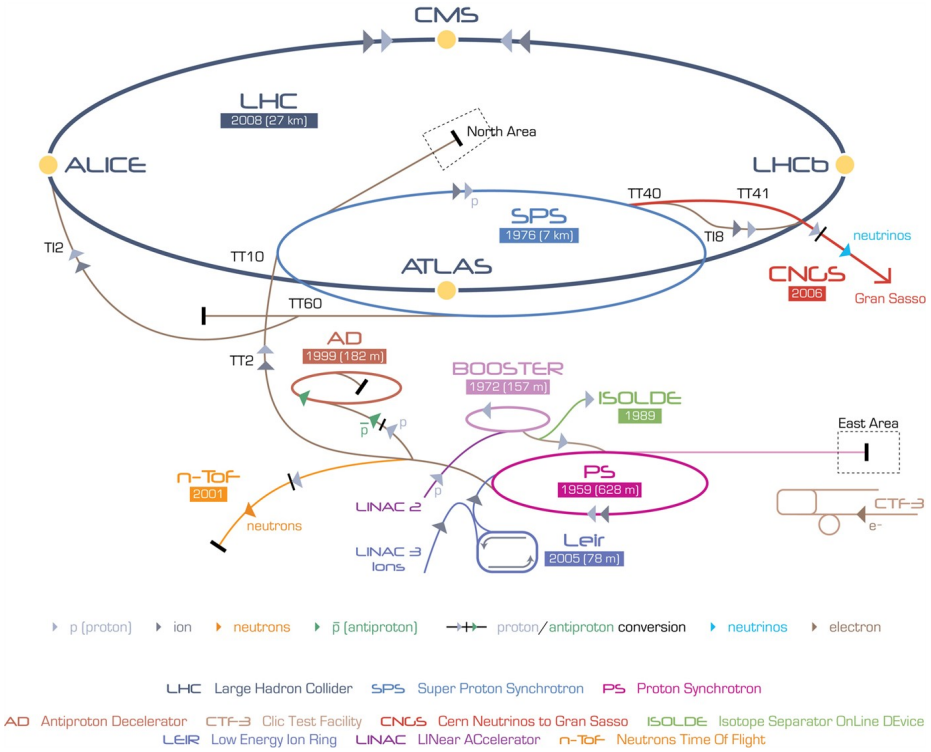

Figure 3.1: Overview of the CERN accelerator complex, including the LHC injector system and surrounding experiments.

The acceleration of the protons is achieved by radio-frequency cavities. These cavities contain a resonant electromagnetic field oscillating at 400 MHz, which is applied to particles passing through. The LHC contains 8 cavities per beam, with each providing a maximum of 2 MV of potential, so each proton can recieve up to 16 MeV of energy per lap. As a result it takes millons of laps over a period of around 20 minutes for a proton injected at 450 GeV to reach its collision energy of 6.5 TeV. These RF cavities also serve to keep each beam in bunches of 1.15×10^{11} protons spaced at intervals of just 25 ns.

The crown jewel of LHC technology is its magnets. 1,232 superconducting NbTi dipole magnets kept at 1.9 K, each spanning 14.3 m and weighing 35 tonnes, create an 8.3 Tesla magnetic. This field lies perpendicular to the beam path, bending it to its desired route. The bending dipole magnets are complemented by 392 quadrupole magnets that focus the beams to a small aperture, and many higher-order multipole magnets which provide small beam corrections.

Allong with the collisional energy of the accelerated particles, the other most important measure of a particle acceletator is the luminosity it achieves. **Luminosity ($\mathcal{L}$)** is used to determine the rate (R) at which a given interaction occurs using:

$$R = \mathcal{L}\sigma \tag{3.1}$$

where σ is the cross-section of the desired interaction. As a result, when searching for rare processes, a obtaining a high luminosity is crucial.

The integrated luminosity, L, gives the total number of interactions over a period of time, and is defined as:

$$L = \int \mathcal{L}\, dt \tag{3.2}$$

At the LHC, the luminosity is controlled by the number of bunches circulating n_b, the frequency of revolution f_r, $N_{1,2}$ the number of particles in each colliding bunch, and the cross sectional area of the colliding beams. This results in the equation:

$$\mathcal{L} = \frac{f_r n_b N_1 N_2}{4\pi\sigma_x\sigma_y} R_\phi \tag{3.3}$$

where R_ϕ is a geometrical loss factor caused by the beams crossing at an angle, and $\sigma_{x,y}$ are the horizontal and vertical widths of the beams, which are estimated to have a Gaussian profile. The LHC currently has a nominal peak luminosity of $\mathcal{L} = 10^{34} cm^{-2} s^{-1}$.

3.2 The ATLAS Experiment

The ATLAS experiment [2] uses the LHC in combination with the general-purpose ATLAS detector to test a broad range of SM and BSM predictions. Together with the CMS experiment, its greatest achievement to date was the detection and discovery of the SM Higgs boson in 2012 [1].

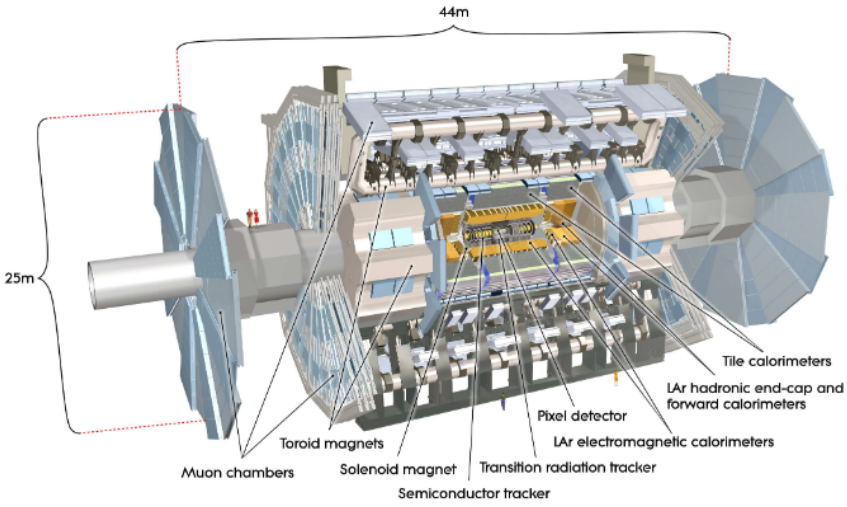

Figure 3.2: A cut-out overview of the ATLAS detector and main components. Diagram from [2].

The ATLAS detector, an overview of which is shown in Figure 3.2, is comprised of several layers, which work in tandem to detect many diverse particles. From innermost to outer-most the layers are:

- the **inner detector**, with excellent angular resolution to track charged particles,
- the **electromagnetic calorimeters**, designed primarily to measure the energy and position of electrons and photons,
- the **hadronic calorimeters** designed to measure the energy and position of hadrons,
- the **muon spectrometer**, to track and measure muons.

When combined with the electronics required to read and trigger on measurements, the entire detector weighs over 7000 t and measures 44 m long by 25 m wide and high. Its barreled shape with end caps covers nearly the full solid angle. The following sections will describe the layout and operations of the ATLAS detector in more detail.

3.2.1 Inner Tracking Detector

The ATLAS inner detector tracks the direction and momentum of charged particles immediately after leaving the interaction point. A 2 T superconducting solenoid surrounds the inner detector, bending charged particles with the Lorentz force, allowing their momentum to be determined from the curvature of their path. Within the inner detector, there are three separate sub-detectors: the **Pixel Detector**, the **Semiconductor Tracker (SCT)**, and the **Transition Radiation Tracker (TRT)**. A cutout view of the detector is shown in Figure 3.3.

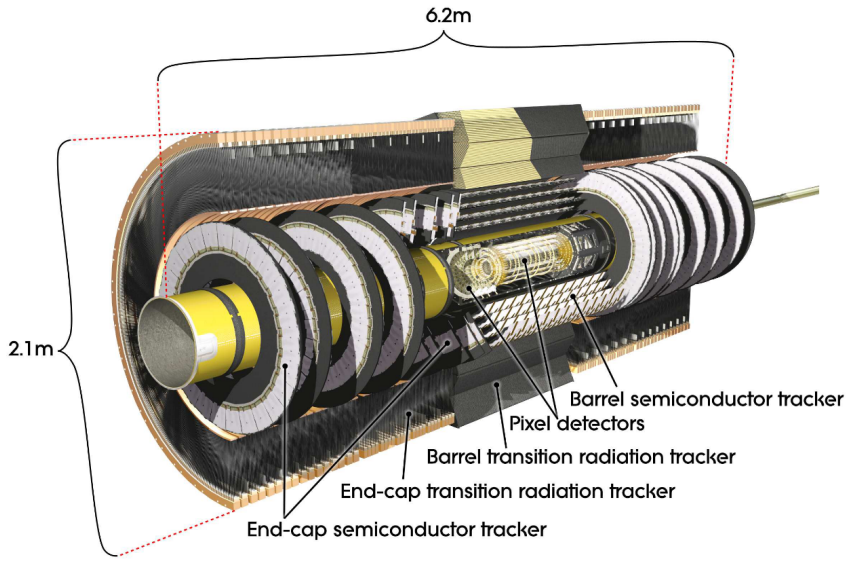

Figure 3.3: A cut-out view of the ATLAS inner detector. Diagram from [2].

The Pixel Detector consists of an array of 1744 pixel sensors, each containing 47232 silicon pixels, mostly measuring 50x400 μm^2. They are arranged into three cyclindrical layers in the barrel and three disk-shaped layers on each end. The high granularity of these detectors ensures strong angular resolution, providing prescise measurements of vertex location and track momentum. Notably, this detector must be very radiation-hard in order to maintain performace over the detector lifespan in an area that recieves an immense radiation dose from the high particle flux.

Though it would be desireable, it would not be feasible to extend the high-resolution pixel detector because of the high cost and signal readout volume. As a result, in the SCT the point-like pixels are extended into silicon strip detectors, which are laid in pairs at an angle of 40 mrad to each other to allow measurements

in two dimensions. The SCT is made up of four concentric cylindrical layers in the barrel and two disk-shaped layers on each end-cap.

The TRT is the final component of the component of the inner detector. It consists of approximately 300000 drift tubes filled with majority Xenon gas, with the walls kept at -1.5 kV and a central wire at ground. When particles pass through the tubes, the gas is ionized and the resulting electrons drift to the centre where the signal is amplified. Additionally, the gaps between TRT straws are filled with polymer fibres (in the barrel) or foils (in the end caps). As a result, highly relativistic particles create transition radiation at the material interfaces, which aids with electron identification.

3.2.2 Calorimeters

The ATLAS calorimeter system measures the energy and positions of both charged and neutral particles after they leave the inner detector. In addition to measuring the energy of particles, the calorimeters must contain enough material to stop the vast majority of particles (with the exception of muons and undetected neutrinos) from reaching the muon spectrometers. To acheive this, high-density passive layers interact with passing particles and cause them to decay into showers, dispersing their energy. These layers are interleaved with active layers that detect the decaying showers to measure particle energy.

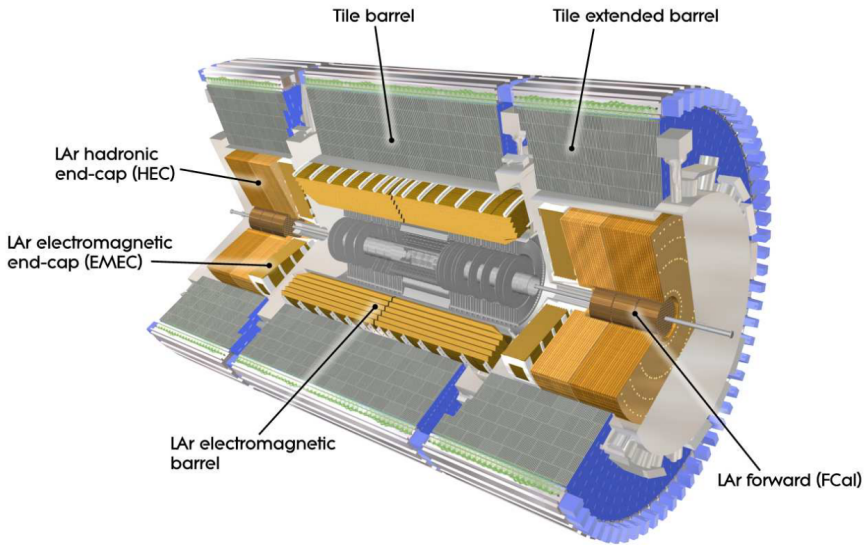

Figure 3.4: A cut-out view of the ATLAS calorimeter system. Diagram from [2].

The ATLAS calorimeters can be categorized into electromagnetic (EM) calorimeters which measure the energy of electrons and photons and hadronic calorimeters which prmarily measure the energy of hadrons. ATLAS uses a combination of two different calorimeter technologies to form these detectors. In the end-cap and forward regions Liquid Argon (LAr) is used as the active layer in both the hadronic and EM calorimeters, while in the barrel region plastic scintillating tiles are employed in the hadronic calorimeter. Figure 3.4 depicts the layout of the ATLAS calorimeter system.

Electromagnetic calorimeters

The electromagnatic LAr calorimeter lies just outside the solenoid surrounding the inner detector. Layers of lead are used as the passive material. In the lead, electrons and photons interact with the closely spaced atoms, initiating a cascading shower of decays. The charged electrons in the shower pass through the active layers and ionize the LAr inside. The electrons and ions then drift across the 2 kV difference to opposite electrodes, where they are amplified into an electrical signal.

Like the inner detector, the LAr EM calorimeter can be divided into an **Electromagnetic Barrel (EMB)** calorimeter and two **Electromagnetic End-Cap (EMEC)** calorimeters. In the barrel region, the layers are placed together in a folded accordion-like geometry to create uniformity and allow easy electronic readout. The barrel and end-cap regions are 53 cm and 63 cm thick respectively, and cover a minimum of 22 and 24 radiation lengths (X_0), keeping shower leakage to a minimum.

Hadronic Calorimeters

In the end cap regions, the **Hadronic End-Cap (HEC)** calorimeter shares a similar design to the EM LAr calorimeters, but with copper as the passive absorbing material between active layers. In the barrel region, the hadronic calorimetry is performed by the **Tile Calorimeter** with plastic scintillators as the active detectors. Particle showers passing through the plastic tiles produce scintillating light, which is directed to photomultipliers to be converted to an electrical signal. In the tile calorimeter, steel is the passive material laid between active layers. The depth of the combination of electromagnetic and hadronic calorimeters is important to prevent particles from punching through to the background-sensitive muon spectrometer. The total thickness, including supporting materials, is approximately 11 interactions lengths,

which keeps punch-through below the levels of irreducible backgrounds in the muon spectrometer and also ensures an accurate measurement of E_T^{miss} as very little energy escapes measurement.

The final calorimeter in the ATLAS detector is the **Forward Calorimeter (FCal)**, located nearest the beam path. It has three layers of passive absorbing metals: an inner copper layer optimized for electromagnetic measurements and two outer tungsten layers to measure hadronic interactions. It too employs liquid argon as the active material, this time in a matrix of longitudinal channels parallel to the beam line.

3.2.3 Muon Spectrometers

After the calorimeters have stopped the vast majority of particles exiting the interaction point, muons and neutrinos remain undetected. The ATLAS experiment does not directly detect neutrinos, and instead reconstructs them from missing transverse momentum, but muons are measured by the muon spectrometer. A diagram of the muon system is shown in Figure 3.5. The centerpiece of this system is an arrangement of three air-core toroidal magnets, a barrel toroid and two end-cap toroids. Each toroid consists of eight coils in loops in a radially symmetric pattern around the beam line. Together they form a 4 T magnetic field to bend muons.

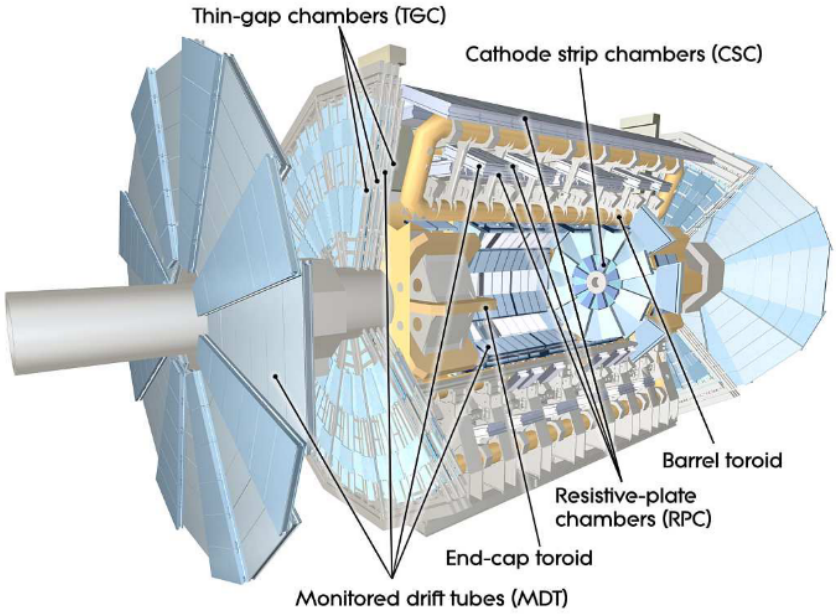

Figure 3.5: A cut-out view of the ATLAS muon spectrometer system. Diagram from [2].

Four different detector types are used to measure the muons. **Monitored Drift Tubes (MDTs)** are pressurized gas drift tubes that collect ionized electrons to measure track coordinates in the bending direction of the magnetic field. They are supplemented by finer-grained and more radiation-hard **Cathode Strip Chambers (CSCs)** at $|\eta| > 2$. **Resistive Plate Chambers (RPCs)** and **Thin Gap Chambers (TGCs)** measure the muon track coordinares in the direction orthogonal to the magnetic bending direction, and are also used by the trigger system to provide bunch-crossing indentification and p_T thresholds.

3.2.4 Trigger and Data Acquisition

The ATLAS detector can see as many as 1.7 billion proton-proton collisions per second, but to save and process all of the information from each collision would require a prohibitive amount of readout electronics, computing power, and storage space. Instead, the trigger system quickly selects events based on key observables to slim down the data. On the detector itself, the **Level-1 (L1) trigger** uses custom electronics within the detector, and works with reduced granularity information from the muon chambers and calorimeters to select potentially interesting events with high-p_T objects or high E_T^{miss}. The detector readout systems can handle a maximum acceptance rate of 100 kHz from the L1 trigger. The **Level 2 (L2) trigger** is outside the detector and uses traditional computing resources. It takes regions of interest where the L1 trigger finds interesting objects and reconstructs them more fully to further reduce the event rate below 3.5 kHz. Together with the L2 trigger, the **event filter** forms the second half of the **High-Level Trigger (HLT)**. At this stage, events are fully reconstructed before being further filtered to a rate of approximately 200 Hz to be analyzed offline.

Chapter 4

Analysis Preparation

4.1 Signal Model

This work concerns a search for dark matter produced in association with a dark Higgs boson as described in Section 2.2.2. The dark Higgs boson then decays to standard model particles with the same branching ratios as a standard model Higgs boson of variable mass, shown in Figure . At low s mass this is dominated by a decay to a pair of b quarks, which has been explored by reinterpreting the ATLAS search for dark matter produced in association with a standard model Higgs boson decaying to $b\bar{b}$. [cite,cite] At s masses above 160 GeV, however, the decay to a pair of W bosons, shown in Figure becomes kinematically available on-shell. Even slightly below this threshold, s decays to WW are the dominant process. The pair of W bosons decay rapidly, and are not detected as final state particles by the ATLAS detector. Instead, they each decay either to hadronic ($q\bar{q}$) or leptonic ($l\nu$) final states. A search in the fully hadronic channel, with both W decaying to $q\bar{q}$ is complete, and this work focuses on the semileptonic decay channel with one $W \to q\bar{q}$ and one $W \to l\nu$. When both analyses are complete, the results will be statistically combined.

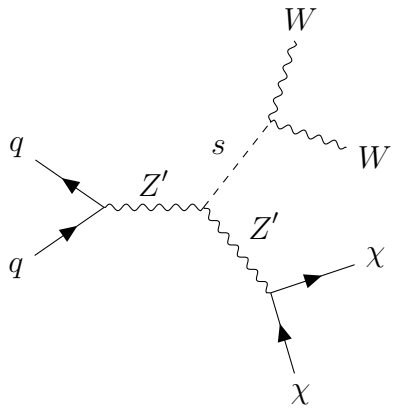

Figure 4.1: DH Decay

In the ATLAS detector this signal signature will be characterized by a single lepton in the final state from the $W \to l\nu$ decay, along with a pair of jets from the $W \to q\bar{q}$ decay and a strong missing transverse energy signature from the dark matter particles and neutrino.

4.2 Monte Carlo Production

Monte Carlo (MC) simulated samples of both BSM (signal) and SM (background) events were used in this analysis. In this way, potentially signal-rich regions can be prepared and studied separately from real data and then later compared to see whether simulated data and true data agree. The following section will detail the signal and background MC samples used.

4.2.1 Signal

Signal samples are produced using the model and parameter choices outlined in Section 2.2.2. They were produced by calculating the hard process cross-section at leading order (LO) using MadGraph5_aMC@NLO 2.7.2 interfaced with Pythia8 8.230 for parton shower modelling. The CKKW-L https://arxiv.org/pdf/1109.4829.pdf procedure with a matching scale of $min(m_s, 40\ GeV)$ was used to prevent overlap between the cross-section matrix element and parton shower. Two separate signal grids were produce, with the second covering an expanded parameter space. In the first, MadGraph5_aMC@NLO was used with the NNPDF23 LO PDF set with $\alpha_s = 0.13$, while in the second MadGraph5_aMC@NLO was both used with the

NNPDF23 LO PDF set with $\alpha_s = 0.13$ and LO QED. The signals studied span a parameter space in m_s and $m_{Z'}$ with samples produced at the mass points shown in Figure . After production, it was found that the second set of samples did not use the ATLAS recommended PDF Set, which is in fact NNPDF23 NLO PDF set with $\alpha_s = 0.118$. When used, the weights of events in these samples are therefore scaled to match the cross-sections of the recommended PDF set.

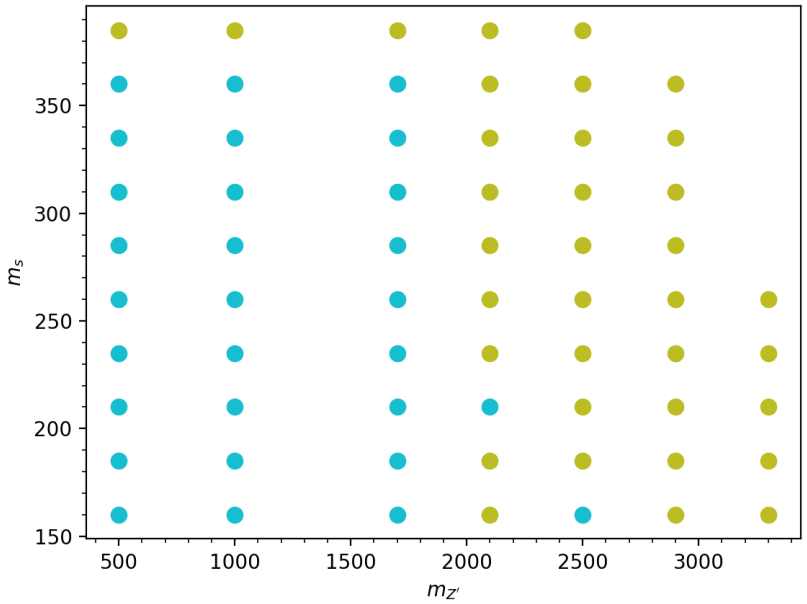

Figure 4.2: Signal point locations in m_s vs. $m_{Z'}$ parameter space.

4.2.2 Background

The dominant SM backgrounds for this analysis are:

- W+jets events a single W boson and 1 or more jets,
- $t\bar{t}$ events with a top and anti-top pair,
- and *Diboson* events with a pair of vector bosons

Additionally, Z+jets and single-top quark (stop) events make non-negligible background contributions. All background contributions are estimated using MC simulated data, and the W+jets and $t\bar{t}$ backgrounds are further constrained using data-driven control regions.

V+jets and diboson

Like signal, two distinct sets of W+jets and Z+jets (V+jets) background samples were used. The samples are similar in that W+jets and Z+jets (V+jets) are simulated with the Sherpa v2.2 MC generator with up to two additional parton emissions at NLO or four additional parton emissions at LO accuracy. Merging of parton showers with matrix elements is acheived using CKKW matching with the MEPS@NLO prescription extending this to NLO. *https://cds.cern.ch/record/2261937/files/ATL-PHYS-PUB-2017-006.pdf* Sect 2.1. The NNPDF30 NNLO https://arxiv.org/pdf/1410.8849.pdf set is used. The difference is that first samples were produced using Sherpa v2.2.1, and the second with Sherpa v2.2.10. As well, additional W+jets samples are added to the second set with $m_W > 120GeV$. This greatly enhances the statistics in this small section of phase space that is important to this analysis. Overlap removal in m_W is performed between these mass-enhanced samples and the other $W+$jets samples. https://cds.cern.ch/record/2753199/files/ATL-COM-PHYS-2021-063.pdf? Diboson samples are similarly generated with only a single set using either Sherpa v2.2.1 or 2.2.2 depending on the process, and CKKW matching again used to merge parton shower and matrix element simulation.

$t\bar{t}$ and single-top

MC samples for the $t\bar{t}$ and single-top standard model background process were modelled using the PowhegBox v2 generator, which gives martix elements at NLO in the strong coupling constant α_s. This uses the NNPDF3.0NO PDF set. Like for signal samples, events were interfaced with Pythia8 8.230 for parton shower modelling using the NNPDF23LO PDF set.

4.3 Object Definition

Once events have been simulated or produced in the ATLAS detector, the information contained in them must be reconstructed into objects which can be analyzed. These objects represent particles or groups of particles and are used to fully or partially reconstruct events and search for signal signatures. The following section will detail the definition of objects used in this analysis.

4.3.1 Muons

From the ATLAS detector, muons are reconstructed from measurements in the Inner Detector and the Muon Spectrometer. For this analysis, two different definitions of muons are used. "*Baseline*" muons use a slighlty less selective reconstruction than "*signal*" muons, which are designed for high purity. *Baseline* muons are selected using the *Loose* identification criteria as defined in https://arxiv.org/pdf/1603.05598.pdf, which is designed to maximize efficiency. *Signal* muons, meanwhile, use the *Medium* identification criteria, and must also be isolated according to the *Tight* track-based working point with variable radius dependent on p_T. Additionally, all muons are rejected if they are considered "badly reconstructed" or "cosmic", and recommended track-to-vertex association cuts are applied. Table 4.1 summarizes the muon selection criteria.

Table 4.1: Muon object definition criteria

Criterion	**Baseline Muon**	**Signal Muon**
Identification	`Loose`	`Medium`
Isolation	-	`TightTrackOnly_VarRad`
Pseudorapidity	$\lvert\eta\rvert < 2.7$	$\lvert\eta\rvert < 2.5$
p_T	$p_T > 7\,\text{GeV}$	$p_T > 7\,\text{GeV}$
Veto	Cosmic or Bad	Cosmic or Bad
Track-to-vertex association	$\lvert d_0/\sigma_{d_0}\rvert < 3$ $\lvert\Delta z_0^{\text{BL}} \sin\theta\rvert < 0.5\,\text{mm}$	$\lvert d_0/\sigma_{d_0}\rvert < 3$ $\lvert\Delta z_0^{\text{BL}} \sin\theta\rvert < 0.5\,\text{mm}$

4.3.2 Electrons

Electrons are reconstructed by associating energy deposits in the EM calorimeter with tracks in the inner detector. Like for muons, two different definitions are used, with "*baseline*" electrons requiring slighlty less selective criteria than "*signal*" electrons. *Baseline* and *signal* electrons are selecteded using a likelihood-based identification described in https://arxiv.org/pdf/1902.04655.pdf. *Signal* electrons require the medium identification criteria, while *baseline* electrons requre the loose criteria as well as a hit in the innermost layer of the pixel detector. Additionally, *baseline* and *signal* electrons must both satisfy the fixed-cut *Loose* isolation requirement. Like for muons, ATLAS recommended track-to-vertex association cuts are applied. Table 4.2

summarizes the electron selection criteria.

Table 4.2: Electron object definition criteria

Criterion	**Baseline Electron**	**Signal Electron**
Identification	`LooseAndBLayerLLH`	`MediumLLH`
Isolation	`FCLoose`	`FCLoose`
Pseudorapidity	$\lvert\eta\rvert < 2.47$	$\lvert\eta\rvert < 2.47$
p_T	$p_T > 7\,\text{GeV}$	$p_T > 7\,\text{GeV}$
Track-to-vertex association	$\left\lvert d_0/\sigma_{d_0}\right\rvert < 5$ $\left\lvert \Delta z_0^{\text{BL}} \sin\theta \right\rvert < 0.5\,\text{mm}$	$\left\lvert d_0/\sigma_{d_0}\right\rvert < 5$ $\left\lvert \Delta z_0^{\text{BL}} \sin\theta \right\rvert < 0.5\,\text{mm}$

4.3.3 Small-radius ($R = 0.4$) Jets

In this analysis, small-R jets are used to reconstruct the hadonically decaying W boson in some analysis regions. Small-R jets are built using particle-flow objects [https://arxiv.org/pdf/1703.10485.pdf] clustered with the anti-k_t algorithm [https://arxiv.org/pdf/0 with radius $R = 0.4$. Following reconstruction, only jets with $pT > 20$ GeV and $|\eta < 2.5|$ GeV are used for analysis. As well, in order to suppress noise from pileup, the jet vertex tagger [https://cds.cern.ch/record/1700870/files/ATLAS-CONF-2014-018.pdf] is applied with the `Tight` working point.

b-jets

For this analysis, it is also beneficial to identify jets originating from bottob (b) quarks. In signal regions these jets are vetoed to reduce background. This is performed using the `DL1r` [https://cds.cern.ch/record/2255226/files/ATL-PHYS-PUB-2017-003.pdf] b-tagging algorithm, which employs a deep-learning neural network. A 77% efficient tagger working point is used. Table 4.3 summarizes $R = 0.4$ jet criteria and tagging.

Table 4.3: $R = 0.4$ jets object definition criteria

Criterion	**Requirement**
Collection	`AntiKt4EMPFlowJets`
Pseudorapidity	$\|\eta\| < 2.5$
p_T	$p_T > 20\,\text{GeV}$
Jet-Vertex-Tagger WP	`Tight`
b-tagger	`DL1r`

4.3.4 Track-Assisted-Reclustered Jets

Track-Assisted-Reclustered (TAR) jets [https://cds.cern.ch/record/2630864] are used in this analysis to reconstruct hadronically decaying W boson candidates in some regions. $R = 0.2$ jets, constructed with the anti-k_t algorithm from locally calibrated topological clusters [https://arxiv.org/abs/1603.02934] are used as input to the TAR algorithm. As well, the TAR algorithm uses tracks fulfilling quality criteria (see Table 4.4). The TAR involves building large-R jets from the constituent small-R jets. Tracks are then matched with the input jets and rescaled using the p_T of the matched jets. The kinematic properties of the TAR jets are then calculated from the constituent $R = 0.2$ jets, while the jet substructure variables are calculated from the constituent tracks. Figure 4.3 shows a visual summary of the base TAR algorithm. The following steps outline the algorithm in more detail:

- Tracks and calibrated anti-k_t $R = 0.2$ jets are chosen as input to the algorithm.
- The anti-k_t $R = 0.2$ jets are reclustered using the anti-k_t algorithm into $R = 1.0$ jets and trimmed using the p_T fraction $f_{cut} = 0.05$.
- Input tracks are matched to $R = 0.2$ jets if possible using ghost association.
- Tracks which remain unassociated are matched to the nearest anti-k_t $R = 0.2$ jet within $\Delta R < 0.3$
- The p_T of each track is rescaled using the p_T of the jet to which it is matched using the equation:

$$p_T^{\text{track, new}} = p_T^{\text{track, old}} \times \frac{p_T^{\text{subjet } j}}{\sum_{i \in j} p_T^{\text{track } i}}, \tag{4.1}$$

where j is the $R = 0.2$ subjet that the track being rescaled is matched with, and the index i runs over all tracks matched to that subjet. This rescaling accounts for the missing neutral momentum, which is measured at calorimeter level but is not present at tracker level.

- Finally, jet substructure variables and m^{TAR} are calculated using the rescaled matched tracks.

The parameters of the TAR algorithm used are summarized in Table 4.4.

Table 4.4: TAR jet reconstruction parameters

Input track selection	`Loose` quality $p_T > 0.5\ GeV$ $\lvert\eta\rvert < 2.5$
Track-to-vertex association	$\lvert d_0\rvert < 2\,\text{mm}$ $\left\lvert \Delta z_0^{\text{BL}} \sin\theta \right\rvert < 3.0\,\text{mm}$
Input jet selection	$R = 0.2$ topo jets $p_T > 20\ GeV$ $\lvert\eta\rvert < 2.5$
Reclustering radius	$R = 1.0$
TAR jet p_T	$p_T^{\text{TAR}} > 100\ GeV$
Trimming radius	$R = 0.2$
Trimming p_T fraction	$f_{\text{cut}} = 0.05$
Track-to-jet association	$\Delta R(\text{jet, track}) < 0.3$

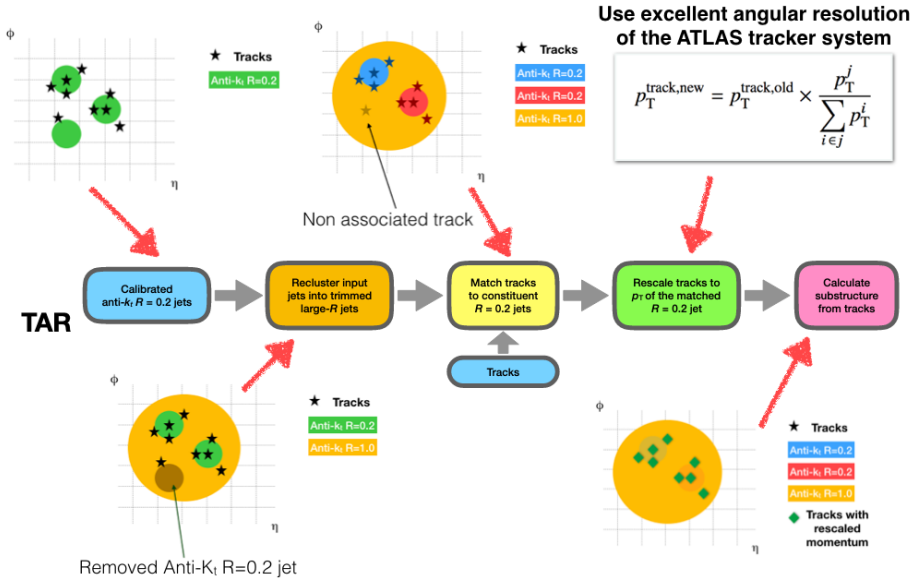

Figure 4.3: A visual summary of the TAR Jet algorithm.

4.3.5 Missing Transverse Momentum (E_T^{miss})

In the ATLAS detector, the beams collide directly along the longitudinal axis. As a result of the conservation of momentum, all decay products from the collision should have a total transverse momentum of 0. As a result, missing transverse momentum (E_T^{miss}) is used to represent undetected objects. In the signal model described in Section 2.2.2 both the neutrino from the leptonically decaying W-boson and the dark matter would not be directly detected in ATLAS. It is impossible to disentangle these objects, and they are reconstructed together using E_T^{miss}. E_T^{miss} is calculated for this analysis using baseline electrons and muons as described in Sections **??** and 4.3.2 as well as $R = 0.4$ jets with the `Tight` working point applied. No photons or τ-leptons are included in the calculation. As well, a soft term is added which is calculated from tracks not associated with the reconstructed objects.

Chapter 5

Evaluation, Analysis and Comparisons

For a Master's research this chapter represents the critical part where **you** are truly evaluated to determine whether you should be given your degree. Even more so for a PhD. Consider carefully what the University calendar states regarding the expectations for a master's thesis, paraphrased here.

1. *A Master's thesis is an original lengthy essay.* The main implication here is that the essay is original, that is, it is completely newly written by you and does not contain any writings from others unless precisely quoted. Any paraphrased items must be cited.

2. *It must demonstrate that:*

    - students understand research methods;
    - students are capable to employ research methods;
    - students demonstrate command of the subject.

3. *The work may be based on:*

    - original data;
    - original exercise from scholarly literature;
    - data by others.

4. *The work must show that:*

- appropriate research methods have been used;
- appropriate methods of critical analysis supplied.

5. *The work must contain:*

   - evidence of some new contribution;
   - evidence of a new perspective on existing knowledge.

Only the last point uses the attribute *new* and it refers almost entirely to giving a new perspective and analysis, even if based on data from others. This truly implies that this current chapter on evaluation and analysis of results is the most important and must be written with care. You are demonstrating here that, even if given data and methods from others, your skills of critical judgment and analysis are now at the level that you can give professional evaluations.

Things are slightly different for a PhD. According to the Graduate Calendar:
a doctoral dissertation must embody original work and constitute a significant contribution to knowledge in the candidate's field of study. It should contain evidence of broad knowledge of the relevant literature, and should demonstrate a critical understanding of the works of scholars closely related to the subject of the dissertation. Material embodied in the dissertation should, in the opinion of scholars in the field, merit publication.

The general form and style of dissertations may differ from department to department, but all dissertations shall be presented in a form which constitutes an integrated submission. The dissertation may include materials already published by the candidate, whether alone or in conjunction with others. Previously published materials must be integrated into the dissertation while at the same time distinguishing the student's own work from the work of other researchers. At the final oral examination, the doctoral candidate is responsible for the entire content of the dissertation. This includes those portions of co-authored papers which comprise part of the dissertation.

The second paragraph makes it clear that one must emphasize what is new and different from others, without arrogance, yet without being too subtle either. The first paragraph implies that for a PhD it is required that one approached an important open problem and gave a new solution altogether, making chapters 3, 4, 5 all part of the body of research being evaluated. In fact at times even the problem may be entirely new, thus including chapter 2 in the examination. This is in contrast to a Master's degree where the minimum requirement is for chapter 5 to be original.

Chapter 6

Conclusions

My first rule for this chapter is to avoid finishing it with a section talking about future work. It may seem logical, yet it also appears to give a list of all items which remain undone! It is not the best way psychologically.

This chapter should contain a mirror of the introduction, where a summary of the *extraordinary* new results and their wonderful attributes should be stated first, followed by an executive summary of how this new solution was arrived at. Consider the practical fact that this chapter will be read quickly at the beginning of a review (thus it needs to provide a strong impact) and then again in depth at the very end, perhaps a few days after the details of the previous 3 chapters have been somehow forgotten. Reinforcement of the positive is the key strategy here, without of course blowing hot air.

One other consideration is that some people like to join the chapter containing the analysis with the only with conclusions. This can indeed work very well in certain topics.

Finally, the conclusions do not appear only in this chapter. This sample mini thesis lacks a feature which I regard as absolutely necessary, namely a short paragraph at the end of each chapter giving a brief summary of what was presented together with a one sentence preview as to what might expect the connection to be with the next chapter(s). You are writing a story, the *story of your wonderful research work*. A story needs a line connecting all its parts and you are responsible for these linkages.

Appendix A

Additional Information

This is a good place to put tables, lots of results, perhaps all the data compiled in the experiments. By avoiding putting all the results inside the chapters themselves, the whole thing may become much more readable and the various tables can be linked to appropriately.

The main purpose of an Appendix however should be to take care of the future readers and researchers. This implies listing all the housekeeping facts needed to continue the research. For example: where is the raw data stored? where is the software used? which version of which operating system or library or experimental equipment was used and where can it be accessed again?

Ask yourself: if you were given this thesis to read with the goal that you will be expanding the research presented here, what would you like to have as housekeeping information and what do you need? Be kind to the future graduate students and to your supervisor who will be the one stuck in the middle trying to find where all the stuff was left!

Bibliography

[1] G. Aad et al. "Observation of a new particle in the search for the Standard Model Higgs boson with the ATLAS detector at the LHC". In: *Physics Letters B* 716.1 (2012), pp. 1–29. ISSN: 0370-2693. DOI: https://doi.org/10.1016/j.physletb.2012.08.020.

[2] G Aad et al. "The ATLAS Experiment at the CERN Large Hadron Collider". In: *JINST* 3 (2008). Also published by CERN Geneva in 2010, S08003. 437 p. DOI: 10.1088/1748-0221/3/08/S08003. URL: https://cds.cern.ch/record/1129811.

[3] John Campbell, Joey Huston, and Frank Krauss. *The black book of quantum chromodynamics: a primer for the LHC era*. Oxford: Oxford University Press, 2018. DOI: 10.1093/oso/9780199652747.001.0001.

[4] Douglas Clowe et al. "A direct empirical proof of the existence of dark matter". In: *Astrophys. J. Lett.* 648 (2006), pp. L109–L113. DOI: 10.1086/508162. arXiv: astro-ph/0608407.

[5] Michael Duerr et al. "Hunting the dark Higgs". In: *JHEP* 04 (2017), p. 143. DOI: 10.1007/JHEP04(2017)143. arXiv: 1701.08780 [hep-ph].

[6] F Englert and R Brout. "Broken symmetry and the masses of gauge vector mesons". In: *Phys. Rev. Lett.* 13 (1964), pp. 321–323. DOI: 10.1103/PhysRevLett.13.321.

[7] "LHC Machine". In: *JINST* 3 (2008). Ed. by Lyndon Evans and Philip Bryant, S08001. DOI: 10.1088/1748-0221/3/08/S08001.

[8] Richard P Feynman. *QED: The Strange Theory of Light and Matter*. Princeton, NJ: Princeton University Press, 2008. ISBN: 9780691164090.

[9] Sheldon L. Glashow. "Partial-symmetries of weak interactions". In: *Nuclear Physics* 22.4 (1961), pp. 579–588. ISSN: 0029-5582. DOI: https://doi.org/10.1016/0029-5582(61)90469-2.

[10] Jeffrey Goldstone, Abdus Salam, and Steven Weinberg. "Broken Symmetries". In: *Phys. Rev.* 127 (3 1962), pp. 965–970. DOI: 10.1103/PhysRev.127.965.

[11] David J Griffiths. *Introduction to elementary particles; 2nd rev. version*. New York, NY: Wiley, 2008.

[12] Particle Data Group et al. "Review of Particle Physics". In: *Progress of Theoretical and Experimental Physics* 2020.8 (Aug. 2020). ISSN: 2050-3911.

[13] Peter W. Higgs. "Broken Symmetries and the Masses of Gauge Bosons". In: *Phys. Rev. Lett.* 13 (1964). Ed. by J. C. Taylor, pp. 508–509. DOI: 10.1103/PhysRevLett.13.508.

[14] Peter W. Higgs. "Spontaneous Symmetry Breakdown without Massless Bosons". In: *Phys. Rev.* 145 (1966), pp. 1156–1163. DOI: 10.1103/PhysRev.145.1156.

[15] M.E. Peskin and D.V. Schroeder. *An Introduction To Quantum Field Theory*. Frontiers in Physics. Avalon Publishing, 1995. ISBN: 9780813345437.

[16] V. C. Rubin, Jr. Ford W. K., and N. Thonnard. "Rotational properties of 21 SC galaxies with a large range of luminosities and radii, from NGC 4605 (R=4kpc) to UGC 2885 (R=122kpc)." In: *Astrophysical Journal* 238 (June 1980), pp. 471–487. DOI: 10.1086/158003.

[17] M.D. Schwartz. *Quantum Field Theory and the Standard Model*. Cambridge University Press, 2014. ISBN: 9781107034730.

[18] Steven Weinberg. "A Model of Leptons". In: *Phys. Rev. Lett.* 19 (21 1967), pp. 1264–1266. DOI: 10.1103/PhysRevLett.19.1264.

[19] F. Zwicky. "On the Masses of Nebulae and of Clusters of Nebulae". In: *Astrophysical Journal* 86 (Oct. 1937), p. 217. DOI: 10.1086/143864.